Towards Tunable Negative-Index Metamaterials

Nicholas P. Montoni,[†] Steven C. Quillin,[†] Charles Cherqui,[†] and David J. Masiello[*,†,‡]

†*Department of Chemistry, University of Washington, Seattle, WA 98195*

‡*Department of Applied Mathematics, University of Washington, Seattle, WA 98195*

E-mail: masiello@chem.washington.edu

Abstract

Ring-like assemblies of metal nanoparticles that exhibit magnetic resonances, called magentic plasmon oligomers, have been of recent interest as negative-index metamaterials. Magnetic plasmon oligomers have potential applications in cloaking, superlensing, information transmission, and sensing. For these reasons, it is imperative to understand the properties of such systems on both small and large scales. We show through theory and simulation that the energy ordering of the magnetic resonances of small oligomers depends greatly on the size and scale of the nanoparticle assembly in ways that purely electric plasmons do not. Following this, we determine the effective pemeability and permittivity of periodic arrays of nanoparticles and show that in certain size regimes they exhibit a negative index of refraction at optical frequencies. As a final exercise, we propose a negative-index material composed of charge tunable semiconductor quantum dots to emphasize the direct control of the optical properties of 2-D magnetic materials.

Keywords

plasmon, hybridization, magnetic, retardation

1 Introduction

Bringing two or more metal nanoparticles (MNPs) together allows their individual electric plasmons to hybridize, producing a new set of plasmonic modes.[1–4] Plasmon hybridization theory is applied to aggregates of MNPs and explains their collective behavior within the quasistatic limit in which the speed of light is taken to be infinite.[5–8] Recently, retardation effects on plasmon hybridization have been the focus of study for large particles[9,10] as well as dimers,[11–13] and 2-D arrays[14–16] of nanoparticles. Specific arrangements of nanoparticles in 2-D arrays, such as three or more nanoparticles arranged on the vertices of a regular polygon, support a collective mode in which all of the dipole plasmons are oriented head-to-tail. This generates a fictitious, oscillating current loop resulting in an oscillating magnetic dipole moment in the center of the ring.[17–22] These so-called magnetic plasmons are the lowest-energy collective modes of the oligomers and couple to and enhance the magnetic field of incident light,[23–25] offering a route to applications such as solar cell enhancement,[26–28] biosensing and detection,[29–36] and information storage and propagation.[37–39] The rich plasmonic modes of magnetic-plasmon-supporting systems are well-described using plasmon hybridization theory, but when in the quasistatic limit, the energy-order of the modes is not.

Plasmon hybridization theory treats plasmons as point dipoles centered on their associated nanoparticles that interact through dipole-dipole coupling. In the quasistatic limit, these dipoles couple only through time-independent, electric near-field interactions,[40] but when the size of and distance between nanoparticles becomes large, this approximation breaks down and intermediate- and far-field effects must be considered, as well as time-delay effects in the near-field.[40] The aim of this paper is to incorporate the fully retarded electric field into plasmon hybridization theory and extend studies of retardation effects to magnetic

plasmon oligomers. Specifically, we begin by exploring oligomers comprising two and three rings of nanoparticles and compare to full-wave simulation[41] to verify that our approach qualitatively predicts the energy-ordering of the magnetic modes.[21,22] Following this, we calaculate the coupling betwen individual rings in various oligomers in order to parametrize an effective magnetic-magnetic coupling between magnetic dipoles. Using this new basis, we describe periodic chains and arrays of oligomers.

The calculations presented here are performed using an electric tight-binding model, parametrizing the magnetic couplings, and then introducing these coupling constants into a magnetic tight-binding model. For all following magnetic oligomers, only the two planar dipoles per particle are considered in the electric tight binding model. The dipoles are mapped onto a set of harmonic oscillators and are described by the following Hamiltonian:

$$H = \sum_{i}^{n} \frac{\mathbf{P}_i^2}{2m_{\mathrm{sp},i}} + \frac{1}{2} m_{\mathrm{sp},i} w_{\mathrm{sp},i}^2 \mathbf{X}_i^2 + e^2 \sum_{i \neq j} \mathbf{X}_i \cdot \mathbf{\Lambda}_{\mathrm{full},ij} \cdot \mathbf{X}_j, \tag{1}$$

where $\mathbf{P}_i$ are the momenta conjugate to the coordinates $\mathbf{X}_i$, $\omega_{sp,i}$ are the individual LSPR frequencies of each oscillator, $m_{sp,i}$ are the LSPR effective masses and $\mathbf{\Lambda}_{\mathrm{full},ij}$ is the fully retarded dipole-dipole relay tensor (expanded below). To make this Hamiltonian more manageable, it is nondimensionalized using $\mathbf{Q}_i = (m_{\mathrm{sp}}\omega_{\mathrm{sp}}/\hbar)^{\frac{1}{2}}\,\mathbf{X}_i$ and $\mathbf{\Pi}_i = \mathbf{P}_i/\sqrt{\hbar m_{\mathrm{sp}}\omega_{\mathrm{sp}}}$. Substituting into Equation 1 and expanding $\mathbf{\Lambda}_{\mathrm{full},ij}$, we get:

$$\begin{aligned} H = \frac{\hbar\omega_{sp}}{2} \sum_{i}^{n} [\mathbf{\Pi}_i^2 + \mathbf{Q}_i^2] - \frac{\hbar\omega_{sp}}{2} \sum_{i \neq j} \{ & g_{ij}^{\mathrm{NF}} \left[3(\mathbf{Q}_i \cdot \hat{\mathbf{n}}_{ij})(\hat{\mathbf{n}}_{ij} \cdot \mathbf{Q}_j) - \mathbf{Q}_i \cdot \mathbf{Q}_j \right] \\ & + g_{ij}^{\mathrm{IF}} \left[3(\mathbf{Q}_i \cdot \hat{\mathbf{n}}_{ij})(\hat{\mathbf{n}}_{ij} \cdot \mathbf{Q}_j) - \mathbf{Q}_i \cdot \mathbf{Q}_j \right] \\ & - g_{ij}^{\mathrm{FF}} \left[(\mathbf{Q}_i \cdot \hat{\mathbf{n}}_{ij})(\hat{\mathbf{n}}_{ij} \cdot \mathbf{Q}_j) - \mathbf{Q}_i \cdot \mathbf{Q}_j \right] \}, \end{aligned} \tag{2}$$

In this Hamiltonian we introduce the near, intermediate, and far-field coupling terms: $g_{ij}^{\mathrm{NF}} = \frac{\alpha_{sp}}{r_{ij}^3} \cos\left(\frac{\omega r_{ij}}{c}\right)$, $g_{ij}^{\mathrm{IF}} = \frac{\alpha_{sp}\omega}{r_{ij}^2 c} \sin\left(\frac{\omega r_{ij}}{c}\right)$, and $g_{ij}^{\mathrm{FF}} = \frac{\alpha_{sp}\omega^2}{r_{ij}c^2} \cos\left(\frac{\omega r_{ij}}{c}\right)$, respectively. Additionally, the polarizability $\alpha_{sp} = \frac{e^2}{m_{sp}\omega_{sp}^2}$, r_{ij} is the distance between the ith and jth LSPs, and $\hat{\mathbf{n}}_{ij}$ is the unit vector connecting two LSPs. Including these terms, we have incorporated all

retardation effects associated with point dipoles.[42]

It should be noted that this Hamiltonian, when diagonilzed, results in a transcendental equation. The eigenvalues of the Hamiltonian are functions of ω, which are the frequencies of the collective modes, that is, the eigenvalues of the eigenvectors. In order to fully solve this problem, we make a first guess of ω for a particular mode of interest and iteratively compute the eigenvalues. Using the eigenvalue associated with the mode of interest, the Hamiltonian is diagonalized to convergence. The process is repeated for each mode of interest.

2 results and discussion

The first systems we examine are a magnetic two-mer,[21] three-mer chain, and three-mer triangle. Because we are interested in the effects of scale, we must define a scaling parameter for the system. Each of our systems begins from a unit cell called the one-mer: six silver, spherical MNPs placed at the corners of a regular hexagon. To create the two-mer, two unit cells are tiled so that they share an edge, and thus two particles. In general, if any two unit cells share an edge, they also share two nanoparticles, as in the diagrams in Figure 1 Each particle has radius a_0 and particles are separated by lattice spacing $r = 2.2 \times a_0$. With the radius of the particles defining the scale of the system, there now exists a way to probe the energy ordering of the modes as a function of size.

The results of our theoretical calculations and full-wave simulations for the aforementioned oligomers are dispayed in Figure 1. Both theory and simulation predict that as a function of size, the energy ordering of the magnetic plasmon modes should change. In the two-mer system, there are two magnetic modes. When the system is small, the lowest energy mode is the alternating north-south (NS) mode and the in-phase north-north mode is highest. When we add a ring to the system, we see a trend emerge. The alternating (NSN) mode is lower than the N-S mode, which is in turn lower than the NNN mode. As a function of size, the modes change order. The triangle system, as a result of its threefold symmetry (as

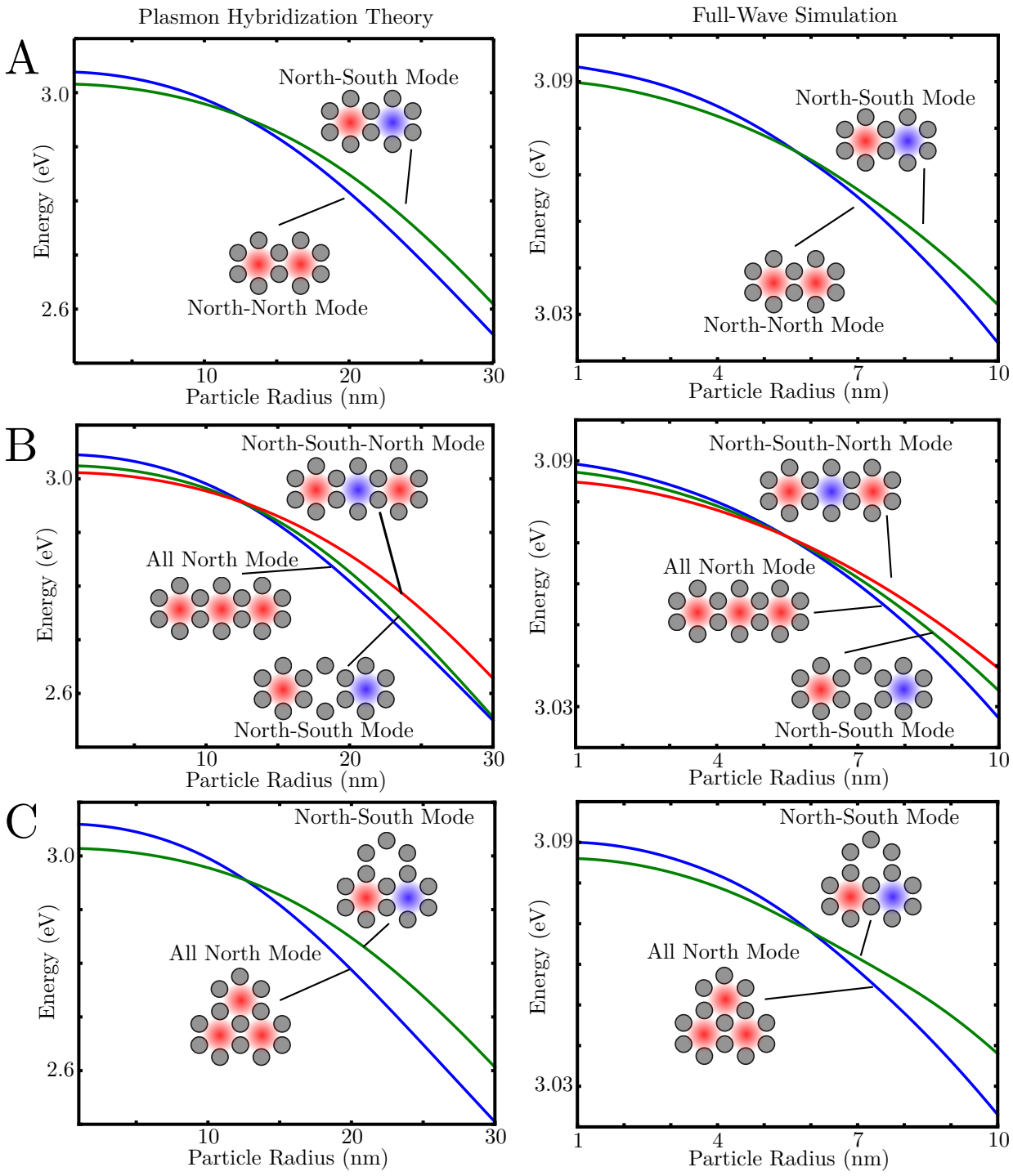

Figure 1: Eigenvalues for the magnetic two-mer (A), three-mer chain (B), and three-mer triangle (C) as computed from the tight binding model (left) and compared to MNPBEM simulations (right). For all three geometries, the net magnetic mode is higher in energy than the net electric mode(s) at small sizes and becomes lower at a certain critical scale value. The tight binding model incorrectly predicts the critical scale value but otherwise is fairly quantitatively accurate.

opposed to twofold for the chains) has slightly different properties. At small size, its lowest energy mode is a pair of degenerate NS modes, while its higher energy mode is an all-north mode. These again switch order as a function of size. In chains with more than three rings, the pattern continues - the magnetic resonances with the most nodes between rings are the lowest energy when small, but the highest when large.

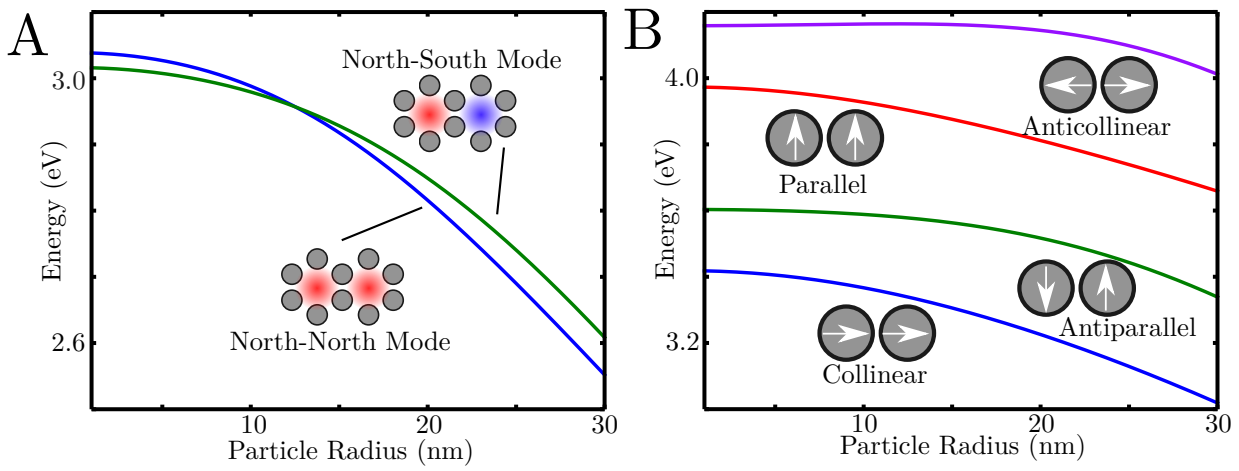

Figure 2: Comparison of the magnetic two-mer (A) and the nanoparticle dimer (B) eigenmodes as a function of scale. Significantly, the two-mer exhibits and change in the energy-ordering of its magnetic modes. However, the nanoparticle dimer does not ever exhibit a change in energy ordering of its eigenmodes. This make energy ordering a uniquely tunable property of fused-ring magnetic oligomers.

This is an unexpected phenomenon. When one considers the energy-order of the four (six) hybridized modes of the nanosphere dimer, it becomes clear that they do not exhibit this effect (Figure 2). Notably, the sphere dimer shows no crossings while the oligomer dimer does. The reason for this outcome is the oligomer dimer's complex structure.[22] The sphere dimer has only one length scale and consitutes only one pairwise interaction. However, the oligomer dimer contains many pairs of nanoparticles over multiple length scales. As a result, different configurations of electric dipoles will be favored at different oligomer sizes, hence the flip of the magnetic modes.

To gain a more visual and intuitive sense of the length scales of each of the terms (near,

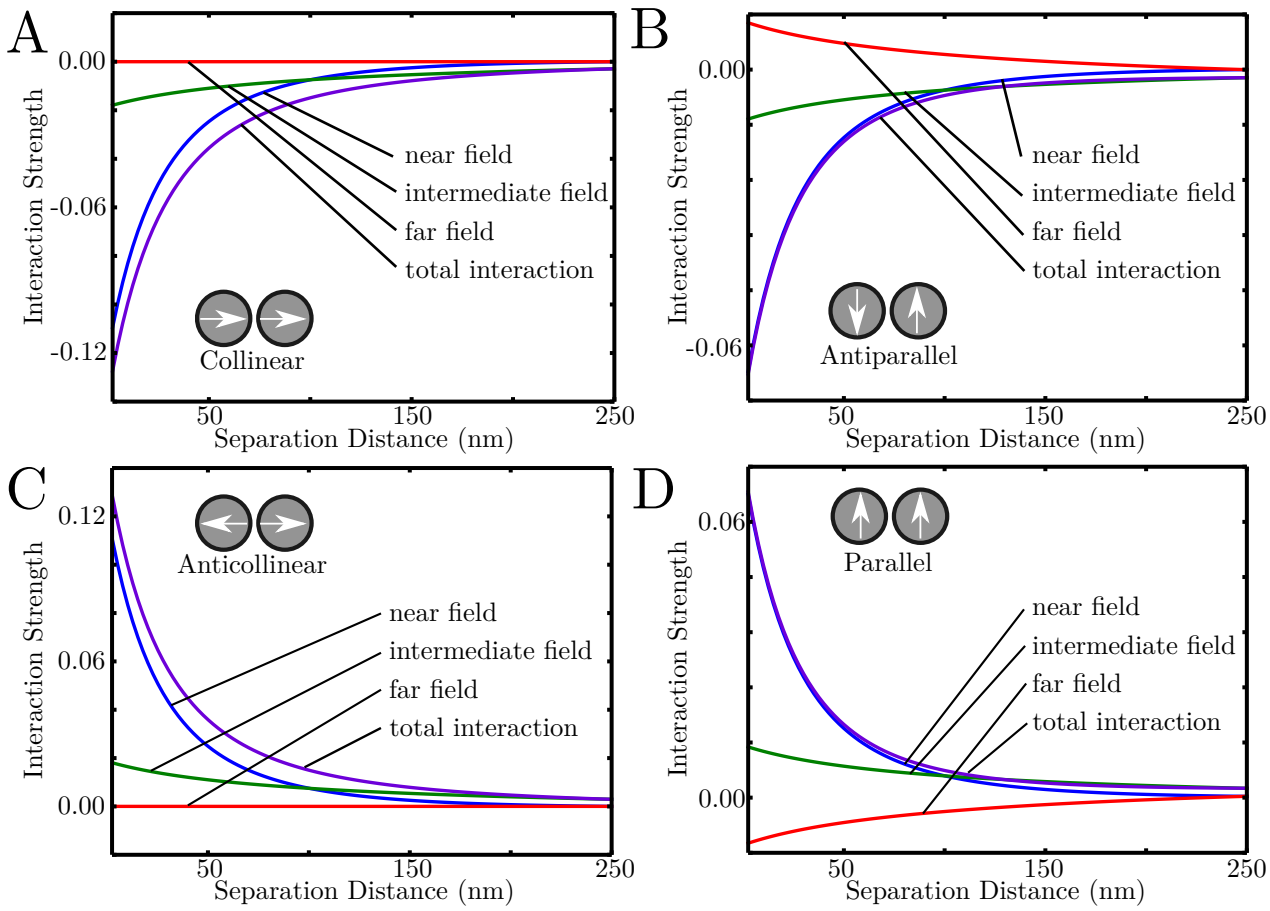

Figure 3: Plots of the interaction terms in the fully retarded electric field for (A) collinear, (B) anti-parallel, (C) anti-collinear, and (D) parallel arrangements of dipoles in a nanoparticle dimer as a function of separation distance. The plots show that at different length scales, different terms in the electric field contribute more to the interaction strength between the particles. As a result, the interactions between one pair of particles in a larger aggregate may be dominated by the interactions between another pair of particles.

intermediate, and far) in the fully retarded electric field of a dipole (found in the coupling terms of Equation 2), we calculated the relative interaction strength between pairs of dipoles (the collective modes of the sphere dimer) as a function of dipole separation distance. The results of these calculations are displayed in Figure 3, showing that at different length scales, different terms in the field contribute more to the energy of the system. Significantly, the interaction strengths display oscillatory motion, which confirms and reinforces past studies on the oscillatory nature of radiation damping.[11]

With a functional and accurate electric dipole tight binding model, we seek a way to simplify our model. Figure 4 displays the eigenvalue curves for three arrangements of two-ring systems, with the rings as (A) nearest neighbors (B) next-nearest neighbors and (C) next-next-nearest neighbors. It is clear that again, at different length scales and relative orientations, the eigenvalue curves behave differently, having different crossing points and energy ordering. Using these eigenvalue curves, the electric dipole model is transformed into a magnetic dipole model. A magnetic dipole is placed at the center of each ring with orientation perpendicular to the plane of the ring. Each dipole has natural frequency ω_{M}, which we determine using the electric tight-binding model for a single ring. The coupling between each magnetic dipole is pulled from the plots in Figure 4 - depending on the spacing between the rings, the dipoles couple through nearest, next-nearest, or next-next-nearest neighbor coupling. The Hamiltonian

$$H = \frac{\hbar\omega_{\mathrm{M}}}{2}\sum_{i}^{n}[\pi_i^2 + q_i^2] + \frac{\hbar\omega_{\mathrm{M}}}{2}\sum_{i\neq j} g_{ij}^{\mathrm{M}} q_i q_j \tag{3}$$

is used in the same way as Equation 2 - diagonalizing it for a set of n magnetic dipoles produces n collective magnetic modes. The benefit of this model is shown by example. For the two-mer, there are ten MNPs, each with two electric dipoles, resulting in twenty collectivel electric modes, two of which were magnetic in character. In the magnetic dipole basis, because there are two rings, there are only two modes - the magnetic modes. This simplifies the data analysis procedures greatly. We find that when the couplings between

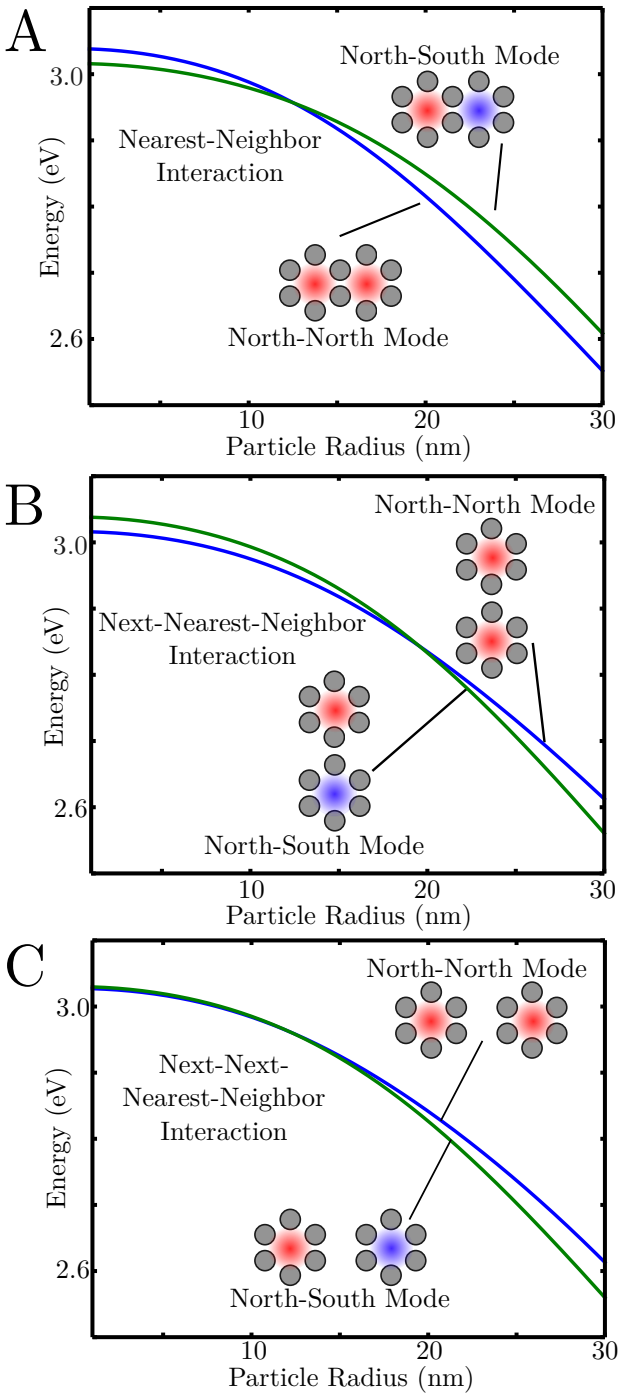

Figure 4: Comparison of coupling schemes for nearest neighbors (A), next-nearest neighbors (B), and next-next nearest neighbors (C) using the electric dipole basis (left) and the magnetic dipole basis parametrized from the electric dipole basis (right). It is clear to see that by parametrizing the coupling between two rings as the difference between the eigenvalues of the NN and NS modes of two rings, we recover exactly the quantitative description provided by the electric dipole basis at much lower computational cost.

rings are parametrized by the differences between the eigenvalues of the dimers in Figure 4, the magnetic dipole Hamiltonian reproduces the results of the electric dipole Hamiltonian exactly. We find, furthermore, that truncating to nearest or next-nearest neighbors in the magnetic dipole model does not lead to any significant loss in quantitative or qualitative agreement between the models. It is this finding that will allow us the extension of the model to larger systems considering only nearest or next-nearest neigbor coupling.

The significant challenge here is to find a colloquial, qualitative, and accurate way to describe extended systems. By considering the magnetic two-mer to be a unit cell of extended systems, the path to characterizing large systems is through a method similar to a two-atom basis molecular tight-binding model. Here, however, the atoms are the rings of the two-mer, and the elements of the hopping matrix are determined by the inter-ring couplings calculated above. More on this model will be presented later.

3 Dielectric Background and a Measure of Quasistaticity

As an additional exercise, and to emphasize the tunability and versatility of magnetic plasmon oligomers, the effect of the dielectric constant of the background (ε_b) is also taken into account. The dielectric constant screens the electric dipoles from each other by effectively weakening their induced electric fields. This means that as ε_b gets large, intermediate and far field effects will weaken in comparison to near field contributions to the electric field. Thus, magnetic plasmon oligomers will be more likely to behave quasistatically when large. In Figure 5A, the difference between the NN and NS modes for magnetic two-mers of four different scaling factors embedded in media with $\varepsilon_b = 1$ to 10 are presented as an example of the impact of screening on the energy ordering of magnetic modes. The results show that when highly screened, even large magnetic plasmon oligomers behave quasistatically.

To extend this to a potential application, we consider now a periodic chain of magnetic monomers - essentially a 1-D system - with only nearest neighbor coupling. When the radii of

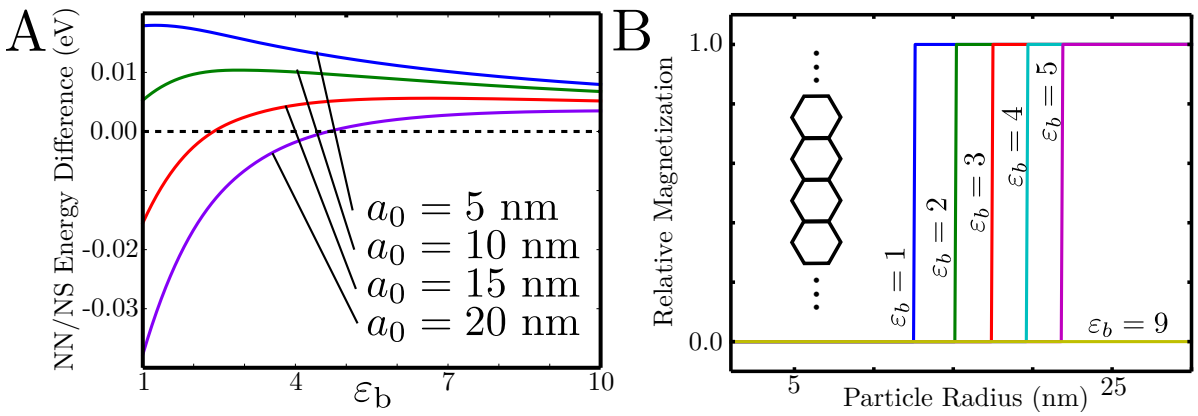

Figure 5: Two measures of the impact of dielectric background on the energy ordering of magnetic modes. In panel A, the difference in energy between the NN and NS modes is plotted for four scale factors as a function of background dielectric constant. This shows that as the dielectric background becomes more opaque, the constituent particles are screened from each other and the two-mer behaves quasistatically. Panel B shows the net magnetization of a periodic chain of six-membered rings at multiple values of epsilon. This again shows that as the constituent particles are screened from each other, the collective behavior becomes more quasistatic. Significantly, this plot also exhibits the property of extended magnetic systems to "turn on" their magnetic response within certain size regimes.

the particles in the chain are small, the lowest energy collective mode of the chain will be an all-alternating magnetic mode, and when the radii are large it will be an all in-phase magnetic mode. A way to quantify this is through a measure of net magnetization. Diagonalizing the magnetic Hamiltonian [reference the equation], summing the eigenvectors, and dividing by n (the number of rings) gives a measure of whether the system is magnetized, and this is plotted as a function of particle radius in Figure 5B. More importantly, the point at which the magnetization "switches on" can be controlled through the dielectric background. This gives rise to the ability of the experimentalist to directly introduce a phase-lag in an extended chain of magnetic oligomers by embedding certain segments of the chain in different materials. This is not so different from certain techniques that are being studied presently in the field[43]

4 Periodic Arrays of Rings - Permeability, Permittivity, and Index of Refraction

To determine the permeability, permittivity, and index of refraction of the six-member ring that is the unit cell, we follow Alu and Engheta.[17] Preparing the magnetic mode of the six-member ring induces a dipole moment on each particle. The dipole moment of a particular particle,

$$\mathbf{p}_i = p\hat{\mathbf{p}}_i = \alpha_{sp}\left(\mathbf{E}_0 + p\sum_{i\neq j}\mathbf{\Lambda_{ij}}\cdot\hat{\mathbf{p}}_i\right) \tag{4}$$

responds to the incident electric field defined by $\nabla\times\mathbf{E}_0 = i\omega\mu_0\mathbf{H}_0$ and the fields scattered by each of the other dipoles. For the magnetic mode, $\mathbf{E}_0 = \frac{i\omega\mu_0 R\mathrm{H}_0}{2}\hat{\mathbf{p}}_i$ with ω the field frequency, N the number of particles in the ring, and μ_0 the background permeability. We are interested in finding the magnetic polarizability, α_M that satisfies $\mathbf{m} = \alpha_M\mathbf{H}_0$, where

$$\mathbf{m} = -\frac{i\omega NRp}{2}\hat{\mathbf{z}} \tag{5}$$

is the magnetic dipole moment of a ring of radius R. From these equations, we find that

$$\alpha_M = \frac{(kR)^2N}{4\varepsilon_b}\left(\frac{\alpha_{sp}}{1-\alpha_{sp}\sum_{i\neq j}\hat{\mathbf{p}}_i\cdot\mathbf{\Lambda}_{ij}\cdot\hat{\mathbf{p}}_j}\right) \tag{6}$$

The effective permeability of a material made of a periodic arrangement of this unit cell is given by $\mu_{\text{eff}} = 1+N_d\left(\alpha_M - i\frac{6\pi}{k^3}\right)$. Here N_d is the number density of rings per unit volume, and $k = \frac{\omega}{c}$ is the wavenumber in the medium.

To compute the effective permittivity of the same ring of nanoparticles, the unit cell is prepared in a uniform electric field. This results in a net dipole moment $\mathbf{p}_E = \sum_{i=1}^{N}\mathbf{p}_i$. The dipole moment on each particle is as above in Eq. 4. Now however, the total dipole moment satisfies $\mathbf{p}_E = \alpha_E\mathbf{E}_0$. This polarizability governs the total electric response of the ring to an electric field, as opposed to the polarizability of a single particle, and is given by

$$\alpha_E = \frac{N\alpha_{sp}}{\left(1 - \alpha_{sp}\sum_{i\neq j}\hat{\mathbf{p}}_i \cdot \mathbf{\Lambda}_{ij} \cdot \hat{\mathbf{p}}_j\right)}. \tag{7}$$

From this polarizability, the effective permittivity of a periodic lattice of this unit cell is $\varepsilon-\text{eff} = 1+N_d\left(\alpha_E - i\frac{6\pi}{k^3}\right)$. The index of refraction of such a material is given by $n = \sqrt{\varepsilon_{\text{eff}}\mu_{\text{eff}}}$ and will take negative values in the frequency range for which both ε_{eff} and μ_{eff} are negative.

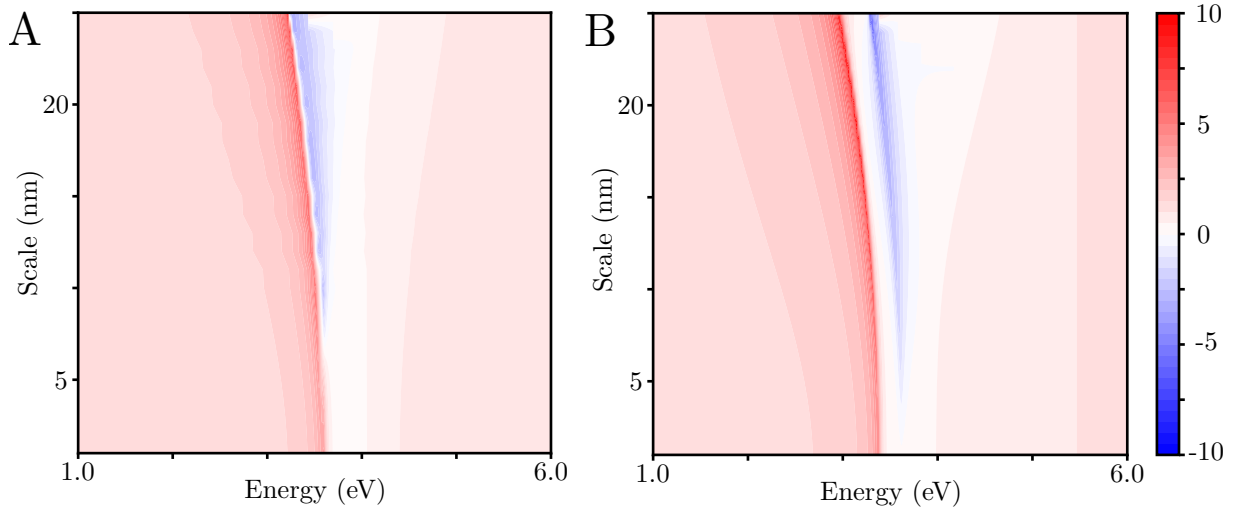

Figure 6: Contour plots of the real index of refraction of a periodic array of one-mer unit cells (A) and two-mer unit cells (B) as a function of energy and scale factor. The blue slices of the plots indicate the regions in which an extended material would exhibit a negative index of refraction.

Extending this concept to more complicated unit cells leads to similar results. Figure 6 shows plots of index of refraction for unit cells composed of one ring (A) and two rings (B) as a function of energy and scale factor. The figures show that at certain sizes materials made of periodic arrays of these unit cells will exhibit a negative index of refraction. This becomes more apparent when a larger unit cell is used, such as the sixmer from Cherqui's work.[21] So far, the model used to determine the index of refraction does not recover the same quantitative accuract as the tight-binding model. However, it offers a powerful qualitative picture to show that a material composed of particles of a certain size will exhibit a negative

index of refraction over a small range of colors.

5 works in progress

I'd like to get plots of the index of refraction as a function of a) ring spacing and b) dielectric background. I think people in the field will care about this.

6 To-do list

Quantum dots: I don't think small, low-density quantum dots have an appreciable magnetic moment, and thus won't have a negative index of refraction. Everything I've computed so far doesn't have a negative index. Let's talk about this. Constructing lenses, calculating transmittance/refelctance: Not sure how to do these calculations or if I should save them for future work. The sixmer: I'd love to talk more about my work with the sixmer. I've computed its indeces of refraction, but I'm not sure how to put all of the information together.

7 Conclusion

It has been shown that magnetic plasmon oligomers are a highly versatile, highly tunable material. The magnetic behavior of tesselated rings of nanoparticles is dependent on size, spacing, arrangement, and environment. Equipped with an understanding of how information propagates along these materials and how to actively influence that information, we are now in a position to study large chains and arrays of magnetic plasmon oligomers. By combining these theoretical studies with existing experimental techniques, there exist ways to directly inlfuence the propagation of information in real time, leading to new applications in detection mechanisms and plamsonic information propagation. Furthermore, we have shown that extended networks of magnetic plasmon oligomers exhibit a negative index of refraction at optical frequencies. Future studies will elucidate the capabilities of materials designed

using the knowledge gained in this exploration.

Acknowledgement

CEI, NSF, DOE, Niket, some other people, probably

References

(1) Clippe, P.; Evrard, R.; Lucas, A. A. Aggregation Effect on the Infrared Absorption Spectrum of Small Ionic Crystals. *Phys. Rev. B* **1976**, *14*, 1715–1721.

(2) Aravind, P.; Nitzan, A.; Metiu, H. The Interaction between Electromagnetic Resonances and its Role in Spectroscopic Studies of Molecules Adsorbed on Colloidal Particles or Metal Spheres. *Surf. Sci.* **1981**, *110*, 189 – 204.

(3) Xu, Y. Electromagnetic Scattering by an Aggregate of Spheres. *Appl. Opt.* **1995**, *34*, 4573–4588.

(4) Mishchenko, M. I.; Mackowski, D. W.; Travis, L. D. Scattering of Light by Bispheres with Touching and Separated Components. *Appl. Opt.* **1995**, *34*, 4589–4599.

(5) Prodan, E.; Radloff, C.; Halas, N. J.; Nordlander, P. A Hybridization Model for the Plasmon Response of Complex Nanostructures. *Science* **2003**, *302*, 419–422.

(6) Prodan, E.; Nordlander, P. Plasmon hybridization in spherical nanoparticles. *J. of Chem. Phys.* **2004**, *120*, 5444–5454.

(7) Nordlander, P.; Oubre, C.; Prodan, E.; Li, K.; Stockman, M. I. Plasmon Hybridization in Nanoparticle Dimers. *Nano Letters* **2004**, *4*, 899–903.

(8) Davis, T. J.; Vernon, K. C.; Gómez, D. E. Designing plasmonic systems using optical coupling between nanoparticles. *Phys. Rev. B* **2009**, *79*, 155423.

(9) Myroshnychenko, V.; Rodriguez-Fernandez, J.; Pastoriza-Santos, I.; Funston, A. M.; Novo, C.; Mulvaney, P.; Liz-Marzan, L. M.; Garcia de Abajo, F. J. Modelling the optical response of gold nanoparticles. *Chem. Soc. Rev.* **2008**, *37*, 1792–1805.

(10) Turner, M. D.; Hossain, M. M.; Gu, M. The Effects of Retardation on Plasmon Hybridization within Metallic Nanostructures. *New J. of Phys.* **2010**, *12*, 083062.

(11) Dahmen, C.; Schmidt, B.; von Plessen, G. Radiation Damping in Metal Nanoparticle Pairs. *Nano Lett.* **2007**, *7*, 318–322, PMID: 17243751.

(12) Rechberger, W.; Hohenau, A.; Leitner, A.; Krenn, J.; Lamprecht, B.; Aussenegg, F. Optical Properties of Two Interacting Gold Nanoparticles. *Opt. Commun.* **2003**, *220*, 137 – 141.

(13) Kottmann, J. P.; Martin, O. J. F. Retardation-Induced plasmon Resonances in Coupled Nanoparticles. *Opt. Lett.* **2001**, 1096–1098.

(14) Haynes, C. L.; McFarland, A. D.; Zhao, L.; Van Duyne, R. P.; Schatz, G. C.; Gunnarsson, L.; Prikulis, J.; Kasemo, B.; Käll, M. Nanoparticle Optics: The Importance of Radiative Dipole Coupling in Two-Dimensional Nanoparticle Arrays. *J. Phys. Chem. B* **2003**, *107*, 7337–7342.

(15) Bouhelier, A.; Bachelot, R.; Im, J. S.; Wiederrecht, G. P.; Lerondel, G.; Kostcheev, S.; Royer, P. Electromagnetic Interactions in Plasmonic Nanoparticle Arrays. *J. Phys. Chem. B* **2005**, *109*, 3195–3198, PMID: 16851340.

(16) Kinnan, M. K.; Chumanov, G. Plasmon Coupling in Two-Dimensional Arrays of Silver Nanoparticles: II. Effect of the Particle Size and Interparticle Distance. *J. Phys. Chem. C* **2010**, *114*, 7496–7501.

(17) Alù, A.; Salandrino, A.; Engheta, N. Negative Effective Permeability and Left-Handed Materials at Optical Frequencies. *Opt. Express* **2006**, *14*, 1557–1567.

(18) Alù, A.; Engheta, N. Dynamical Theory of Artificial Optical Magnetism Produced by Rings of Plasmonic Nanoparticles. *Phys. Rev. B* **2008**, *78*, 085112.

(19) Hentschel, M.; Dregely, D.; Vogelgesang, R.; Giessen, H.; Liu, N. Plasmonic Oligomers: The Role of Individual Particles in Collective Behavior. *ACS Nano* **2011**, *5*, 2042–2050, PMID: 21344858.

(20) Brandl, D. W.; Mirin, N. A.; Nordlander, P. Plasmon Modes of Nanosphere Trimers and Quadrumers. *J. Phys. Chem. B* **2006**, *110*, 12302–12310.

(21) Cherqui, C.; Bigelow, N. W.; Vaschillo, A.; Goldwyn, H.; Masiello, D. J. Combined Tight-Binding and Numerical Electrodynamics Understanding of the STEM/EELS Magneto-Optical Responses of Aromatic Plasmon-Supporting Metal Oligomers. *ACS Photonics* **2014**, *1*, 1013–1024.

(22) Cherqui, C.; Wu, Y.; Li, G.; Quillin, S. C.; Busche, J. A.; Thakkar, N.; West, C. A.; Montoni, N. P.; Rack, P. D.; Camden, J. P. .; Masiello, D. J. STEM/EELS Imaging of Magnetic Hybridization in Symmetric and Symmetry-Broken Plasmon Oligomer Dimers and All-Magnetic Fano Interference. *Nano Lett.* **2016**, *16*, 6668–6676, PMID: 27673696.

(23) Shalaev, V. M. Optical negative-index metamaterials. *Nat. Photonics* **2007**, *1*, 41–48.

(24) Qian, Z.; Hastings, S. P.; Li, C.; Edward, B.; McGinn, C. K.; Engheta, N.; Fakhraai, Z.; Park, S.-J. Raspberry-like Metamolecules Exhibiting Strong Magnetic Resonances. *ACS Nano* **2015**, *9*, 1263–1270.

(25) Urzhumov, Y. A.; Shvets, G.; Fan, J. A.; Capasso, F.; Brandl, D.; Nordlander, P. Plasmonic Nanoclusters: a Path towards Negative-Index Metafluids. *Opt. Express* **2007**, *15*, 14129–14145.

(26) Graydon, O. Solar cells: Fano-enhanced performance. *Nat. Photonics* **2011**, *6*, 4.

(27) Le, K. Q.; Alu, A. Fano-Induced Solar Absorption Enhancement in Thin Organic Photovoltaic Cells. *Appl. Phys. Lett.* **2014**, *105*, 141118.

(28) Le, K. Q.; Bai, J. Enhanced Absorption Efficiency of Ultrathin Metamaterial Solar Absorbers by Plasmonic Fano Resonance. *JOSA B* **2015**, *32*, 595–600.

(29) Karaveli, S.; Zia, R. Strong Enhancement of Magnetic Dipole Emission in a Multilevel Electronic System. *Opt. Lett.* **2010**, *35*, 3318–3320.

(30) Noginova, N.; Zhu, G.; Mavy, M.; Noginov, M. Magnetic Dipole Based Systems for Probing Optical Magnetism. *J. Appl. Phys.* **2008**, *103*, 07E901.

(31) Wang, J.; Fan, C.; He, J.; Ding, P.; Liang, E.; Xue, Q. Double Fano Resonances Due to Interplay of Electric and Magnetic Plasmon Modes in Planar Plasmonic Structure with High Sensing Sensitivity. *Opt. Express* **2013**, *21*, 2236–2244.

(32) Zhu, Z.; Bai, B.; You, O.; Li, Q.; Fan, S. Fano Resonance Boosted Cascaded Optical Field Enhancement in a Plasmonic Nanoparticle-in-Cavity Nanoantenna Array and its SERS Application. *Light: Science and Applications* **2015**, *4*, e296.

(33) Lee, K.-L.; Huang, J.-B.; Chang, J.-W.; Wu, S.-H.; Wei, P.-K. Ultrasensitive Biosensors Using Enhanced Fano Resonances in Capped Gold Nanoslit Arrays. *Scientific Reports* **2015**, *5*, 8547.

(34) Wu, C.; Khanikaev, A. B.; Adato, R.; Arju, N.; Yanik, A. A.; Altug, H.; Shvets, G. Fano-Resonant Asymmetric Metamaterials for Ultrasensitive Spectroscopy and Identification of Molecular Monolayers. *Nat. Mat.* **2012**, *11*, 69–75.

(35) Cetin, A. E.; Altug, H. Fano Resonant Ring/Disk Plasmonic Nanocavities on Conducting Substrates for Advanced Biosensing. *ACS Nano* **2012**, *6*, 9989–9995.

(36) Zhang, S.; Bao, K.; Halas, N. J.; Xu, H.; Nordlander, P. Substrate-Induced Fano Resonances of a Plasmonic Nanocube: a Route to Increased-Sensitivity Localized Surface Plasmon Resonance Sensors Revealed. *Nano Lett.* **2011**, *11*, 1657–1663.

(37) Liu, H.; Genov, D. A.; Wu, D. M.; Liu, Y. M.; Steele, J. M.; Sun, C.; Zhu, S. N.; Zhang, X. Magnetic Plasmon Propagation Along a Chain of Connected Subwavelength Resonators at Infrared Frequencies. *Phys. Rev. Lett.* **2006**, *97*, 243902.

(38) Liu, N.; Mukherjee, S.; Bao, K.; Brown, L. V.; Dorfmüller, J.; Nordlander, P.; Halas, N. J. Magnetic Plasmon Formation and Propagation in Artificial Aromatic Molecules. *Nano Lett.* **2011**, *12*, 364–369.

(39) Liu, N.; Mukherjee, S.; Bao, K.; Li, Y.; Brown, L. V.; Nordlander, P.; Halas, N. J. Manipulating Magnetic Plasmon Propagation in Metallic Nanocluster Networks. *ACS Nano* **2012**, *6*, 5482–5488.

(40) Jackson, J. D. *Classical Electrodynamics*, 3rd ed.; Wiley: New York, NY, 1999.

(41) Hohenester, U.; Trügler, A. MNPBEM - A Matlab Toolbox for the Simulation of Plasmonic Nanoparticles. *Comp. Phys. Comm.* **2012**, *183*, 370 – 381.

(42) Purcell, E. M.; Pennypacker, C. R. Scattering and Absorption of Light by Nonspherical Dielectric Grains. *Astrophys. J.* **1973**, *186*, 705–714.

(43) Yang, A.; Hoang, T. B.; Dridi, M.; Deeb, C.; Mikkelson, M. H.; Schatz, G. C.; Odom, T. W. Real-time tunable lasing from plasmonic nanocavity arrays. *Nature Comm.* **2015**, *6*, 6939.

Graphical TOC Entry

Some journals require a graphical entry for the Table of Contents. This should be laid out "print ready" so that the sizing of the text is correct.
Inside the `tocentry` environment, the font used is Helvetica 8 pt, as required by *Journal of the American Chemical Society*.
The surrounding frame is 9 cm by 3.5 cm, which is the maximum permitted for *Journal of the American Chemical Society* graphical table of content entries. The box will not resize if the content is too big: instead it will overflow the edge of the box.
This box and the associated title will always be printed on a separate page at the end of the document.